NANO LETTERS

Letter

pubs.acs.org/NanoLett

Increased Responsivity of Suspended Graphene Photodetectors

Marcus Freitag,* Tony Low, and Phaedon Avouris

IBM T.J. Watson Research Center, Yorktown Heights, New York 10598, United States

ABSTRACT: The responsivity of graphene photodetectors depends critically on the elevated temperature of the electronic subsystem upon photoexcitation. We investigate the role of the substrate in providing cooling pathways for photoexcited carriers under ambient conditions by partially suspending few-layer graphene over a trench. Through photocurrent microscopy, we observe p−n junctions near the supported/suspended interfaces that produce photothermoelectric currents. Most importantly, we find the photocurrent in suspended p−n junctions to be an order of magnitude larger than in supported structures. This enhancement is attributed to the elimination of a dominant electronic cooling channel via the surface phonons of the polar substrate. Our work documents this mechanism of energy exchange between graphene and its environment, and it points to the importance of dielectric engineering for future improved graphene photodetectors.

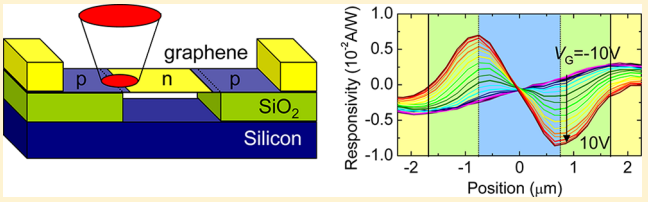

KEYWORDS: *Graphene, photodetector, p−n junction, hot electron, surface polar phonon, electron cooling*

Graphene photosensors based on bolometric,[1−3] thermoelectric,[4−7] or photovoltaic[3,8−11] effects have recently been demonstrated. The advantages of graphene in these applications include a bandwidth as high as 500 GHz[9,12,13] and photosensitivity to long-wavelength radiation in the THz or mid-IR. A key characteristic of superefficient optoelectronic devices is the utilization of the excess energy of photoexcited carriers before it is lost to the phonon bath, for example through carrier multiplication[14] or generation of hot electrons.[15] Graphene's strong bonding implies large optical phonon energies. Its high Fermi velocity and linear dispersion implies limited scattering phase space for acoustic phonons.[16−20] These properties underlie the very weak electron−phonon coupling in graphene when compared to other material systems. As a result, upon carrier excitation with light or other means, the electronic temperature in graphene can be driven far from equilibrium with potential for efficient optoelectronic devices. However, in comparison with other materials, graphene presents a unique situation, since its dominant electronic cooling mechanism can be extrinsic, rather than the typical electron interaction with internal phonon modes. For example, electrical contacts attached to graphene may serve as an efficient heat bath for the hot electrons. Impurities and other defects can serve to relax the momentum conservation constraint in electron scattering with acoustic phonons, leading to larger scattering phase space.[21,22] Graphene being a two-dimensional membrane also interacts intimately with its underlying substrate. For example, substrate surface polar phonons (SPPs) which are present in common substrates such as SiO_2 and h-BN may provide additional electron energy decay channels.[23−25] In fact, these SPPs generally have lower energies than the graphene internal optical phonons, and they couple strongly with the electronic degrees of freedom in graphene.[23−26]

Here, we present photocurrent measurements on partially suspended few-layer graphene, where we can test the role of the substrate in cooling the photoexcited electrons. The photocurrent maximum occurs close to the suspended-supported graphene interface, that is, the position of the p−n junction. We find close to an order of magnitude increase in photocurrent compared to usual substrate-supported graphene p−n junctions under room temperature conditions. This increase cannot simply be explained by a reduced phononic heat conduction into the gate stack. Instead, the charge carriers attain an order of magnitude higher electron temperature due to the absence of electron-SPP scattering. The response to gate bias shows that the photocurrent is due to a thermoelectric effect,[4−7] as opposed to the photovoltaic effect which dominates in graphene on a uniform SiO_2 dielectric.[10,11] These results clearly show that the role of substrate phonons cannot be neglected in estimating the thermoelectric photocurrent in supported graphene.

Our graphene photodetector, consisting of three layers of graphene partially suspended over a trench and contacted by metal contacts, is shown in Figure 1a. Few-layer graphene was mechanically exfoliated from graphite on silicon substrates with 300nm SiO_2 and prefabricated trenches 300 nm deep and 1.3 μm wide. The layer number was determined by the reduction of the silicon Raman signal due to the graphene overlayer. Metal contacts were subsequently defined by e-beam lithography, metal deposition, and lift-off. As-prepared, the graphene exhibited p-type behavior. Very gentle annealing with currents[27] on the order of 30 μA (corresponding to an electrical power on the order of 1 μW) and simultaneous raster-scanning of light of 100 μW power and λ = 476.5 nm wavelength lead to

Received: January 9, 2013
Revised: February 15, 2013
Published: March 1, 2013

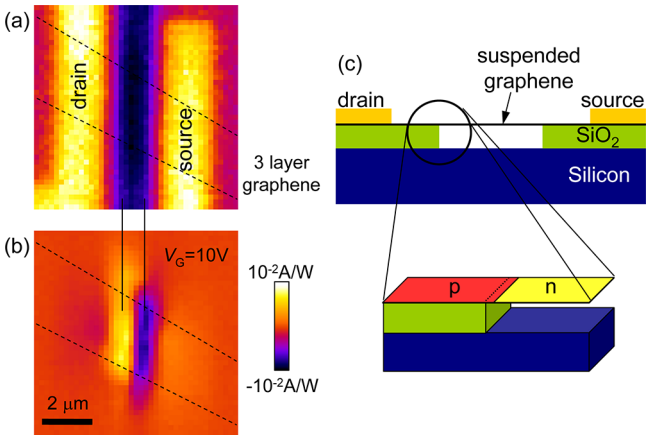

Figure 1. Partially suspended graphene p−n−p junction. (a) Reflected laser light image of the device, showing the contacts, the SiO_2 support, and the trench. A three-layer graphene flake is exfoliated on top of the structure as indicated by dashed lines. (b) Spatially resolved responsivity of the graphene photodetector, measured with wavelength λ = 514.5 nm and backgate voltage V_G = 10 V. A peak responsivity on the order of 10^{-2} A/W is measured near the suspended-supported interface. (c) Schematic of the device, showing two 1 μm long supported graphene segments and the 1.5 μm long suspended part. The trench depth is 300 nm. The supported part is heavily p-doped by the substrate, while the suspended part is only lightly doped after annealing and can be switched n-type or p-type by a gate voltage. The p−n junction is located about 100 nm inside the suspended part due to electrostatics.

an ambipolar gate-voltage characteristic due to selective removal of dopants in the suspended part. We found that it was important to apply both the current and the light simultaneously to achieve efficient removal of dopants in the suspended part. The supported part stayed unaffected at these low power levels. Application of a gate voltage leads to asymmetrical electrostatic doping in the suspended and supported parts due to the different dielectric constants of SiO_2 and air, thus creating two back-to-back p−n junctions at the suspended/supported interfaces. For the photoconductivity experiments, we illuminate the sample with focused laser light of 514.5 or 476.5 nm wavelength and about 500−800 nm spot size. The laser spot is raster-scanned across the sample while the photocurrent is recorded, thus generating spatially resolved images of the photocurrent together with images of the back-reflected light to locate the electrodes and trench (Figure 1).

We first consider the two possible photocurrent generation mechanisms, photovoltaic (PV) and thermoelectric (TE). In previous works, the PV effect has been found to dominate in graphene p−n junctions supported on SiO_2,[10,11] while the TE effect dominates in graphene p−n junctions with top-gate dielectrics of h-BN.[6] In our partially suspended p−n junctions, the supported part is p-doped, and even though the gate-channel coupling is strong due to the dielectric constant ε = 3.9 of SiO_2, we do not reach the Dirac point in supported graphene even at the highest applied gate voltage of V_G = 10 V due to the substrate doping. In contrast, the suspended part is close to being intrinsic due to the removal of dopants through current annealing and the absence of substrate doping, thus allowing us to switch between bipolar p−n−p and unipolar p^+−p−p^+ conditions as shown in Figure 2b. To unambiguously differentiate between the two mechanisms, we follow refs 6 and 7 and use the direction of the photocurrent in the cases of bipolar p−n junctions and unipolar p^+p junctions as the diagnostic (first index supported part, second index suspended part). In the case of a dominant PV effect, these combinations should lead to photocurrents in the same direction, while in the case of the TE mechanism the photocurrent should reverse sign in the unipolar junction. Figure 2 shows that the photocurrent clearly switches sign between these conditions, and the signs are consistent with the TE effect. A sign change for the PV effect would require to switch the electric field direction and go from pn, p^+p, nn$^-$ on the one hand to np, pp$^+$, n$^-$n on the other. The stronger coupling to the backgate on the supported part together with the intrinsic p-doping of the supported part, does not allow biasing the device in either np or pp$^+$ conditions. The electric field could only reverse when the region in the supported part becomes more n-type than in the suspended part (n$^-$n), but since the supported part stays p-type at V_G = 10 V, this is not possible. Even if we could push the gate voltage higher without damaging the suspended graphene, the switch in PV photocurrent would have the wrong sign. We have thus established the dominance of the thermoelectric effect in partially suspended samples.

The responsivity of our suspended graphene photodetector under room temperature conditions, ~1 × 10^{-2} A/W, is about an order of magnitude larger than that of fully supported devices based also on the thermoelectric effect (Table 1).[4−6,13]

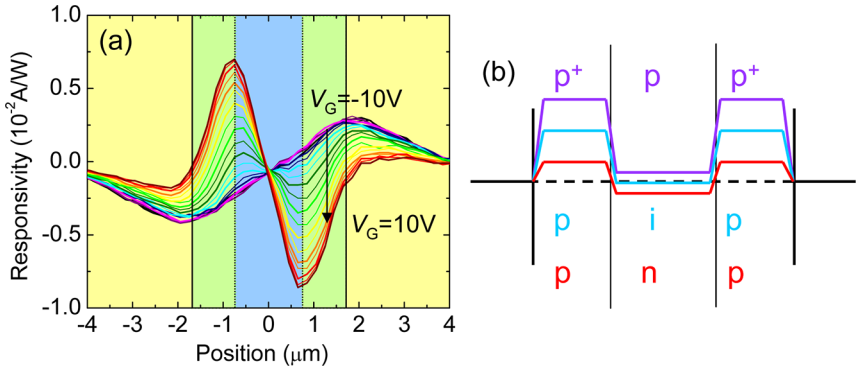

Figure 2. Photoresponse of the partially suspended graphene device. (a) Responsivity as a function of position for various gate voltages. Peak responsivity occurs at the highest positive gate voltage. The laser wavelength was λ = 476.5 nm and the incident laser power P = 100 μW. (b) Schematic of the back-to-back junctions as a function of gate voltage. At V_G = 10 V an ambipolar p−n−p junction exists, while at V_G = −10 V a unipolar p^+−p−p^+ junction is present.

dx.doi.org/10.1021/nl4001037 | Nano Lett. 2013, 13, 1644−1648

Table 1. Comparison of the Sensitivity of Our Suspended Graphene Photodetector with Substrate-Supported Graphene Photodetectors Taken from the Literature[a]

type	temp.	power	λ	current	responsivity per layer
this work: suspended trilayer	300 K	100 μW	476 nm	800 nA	2.7e^{-3} A/W
ref 4: SLG-BLG junction	12 K	40 μW	635 nm	40 nA	6.7e^{-4} A/W
ref 4: SLG-BLG junction	300 K	40 μW	635 nm	3 nA	5e^{-5} A/W
ref 5: p−n junction	300 K	40 μW	600 nm	10 nA	2.5e^{-4} A/W
ref 5: bilayer p−n junction	300 K	30 μW	532 nm	45 nA	7.5e^{-4} A/W
ref 6: p−n junction	40 K	50 μW	850 nm	40 nA	8e^{-4} A/W
ref 6: bilayer p−n junction	40 K	200 μW	850 nm	30 nA	7.5e^{-5} A/W
ref 13: p−n junction	20 K	70 μW	800 nm	200 pA	3e^{-6} A/W

[a]The photocurrent generation mechanisms are based on the thermoelectric effect throughout. The responsivity values are normalized to the incident laser power and graphene layer number. For SLG-BLG junctions we normalized with the average 1.5 layers.

The enhanced photothermoelectric current indicates a higher carrier electronic temperature. A possible explanation is the partial elimination of a dominant electronic cooling channel via the SPP due to the polar SiO_2 substrate.[23−25,28] Indeed, the SiO_2 SPPs which have lower energies (60 and 150 meV) than the intrinsic graphene optical phonons (160 and 200 meV) are expected to be involved in the dominant power loss mechanism under ambient temperature and moderate doping conditions.[25] Calculations of the SPP electronic cooling yield an "out-of-plane" thermal conductance (i.e., from the electron subsystem to the phonon subsystem) of γ_e = 1−10 MW/m^2·K, while that due to intrinsic phonons is an order of magnitude smaller.[25] Hence, the overall reduction in the out-of-plane thermal conductance in our partially suspended graphene devices would result in a higher electronic temperature. In what follows, we perform the following analysis: (i) First, making use of the knowledge of the out-of-plane thermal conductance in our partially suspended graphene device, we estimate its electronic temperature by solving the heat transport equation. (ii) Second, we extract the device electronic temperature "experimentally", since the measured photothermoelectric current serves as a "thermometer" of the device's electronic temperature. These two approaches for extracting the electronic temperature are then compared and discussed.

Upon light illumination, the electronic temperature of graphene (T_e) achieves a steady-state elevated temperature with respect to the ambient (T_0 = 300 K). The spatial profile of T_e depends on many factors, such as the device geometry, laser power profile, and electronic coupling to the phonon baths and the metallic contacts. It can be modeled by the following differential heat equation,

$$-h\kappa_e\frac{d^2T_e}{dx^2} + \gamma_e(x)(T_e - T_0) = P(x) \quad (1)$$

$h \approx 1$ nm is the thickness of trilayer graphene. κ_e is the in-plane electronic thermal conductivity, which we estimate through the Wiedemann−Franz relation from our device's electrical conductivity to be ≈1 W/m·K. Electrons in graphene can couple to both the internal and substrate polar phonons, and the electronic heat dissipation efficiency is described by an out-of-plane thermal conductance given by γ_e. In this work, a value of $\gamma_e \approx 5$ MW/m^2·K and $\gamma_e \approx 0.5$ MW/m^2·K on the supported and suspended regions respectively is employed.[25] The supported region is a more efficient "cooling pad" since the electrons can couple to both the internal and substrate surface polar phonons.[25] $P(x)$ is the spatial profile of the light illumination on graphene, which we assume to be Gaussian,

$$P(x) = \frac{\alpha P_0}{\sigma_0 L_{spot}\sqrt{2\pi}}\exp\left[-\frac{(x-x_0)^2}{2\sigma_0^2}\right] \quad (2)$$

where α is the absorption coefficient for trilayer graphene, taken to be ≈ 7%, and $P_0 \approx 100$ μW is the laser power. The laser spot size, taken to be the half-width of the Gaussian profile, is given by $L_{spot} = 2(2\ln 2)^{1/2}\sigma_0 \approx 0.5$ μm and x_0 denotes the position of the peak laser intensity.

We solved eq 1 numerically to obtain the spatial profile of the electronic temperature as shown in Figure 3b,c, for partially suspended and fully supported graphene devices respectively. In the former, the length of the trench is $L \approx 1.5$ μm and the supported regions are ≈ 1 μm, as illustrated in Figure 3a. A maximum elevated temperature of $\delta T = T_e - T_0 \approx 40$ K was obtained at the supported-suspended interface (i.e., $x = 0$). Further away from the supported region (i.e., $x > 100$ nm), a maximum elevated temperature of $\delta T \approx 50$ K was obtained. On

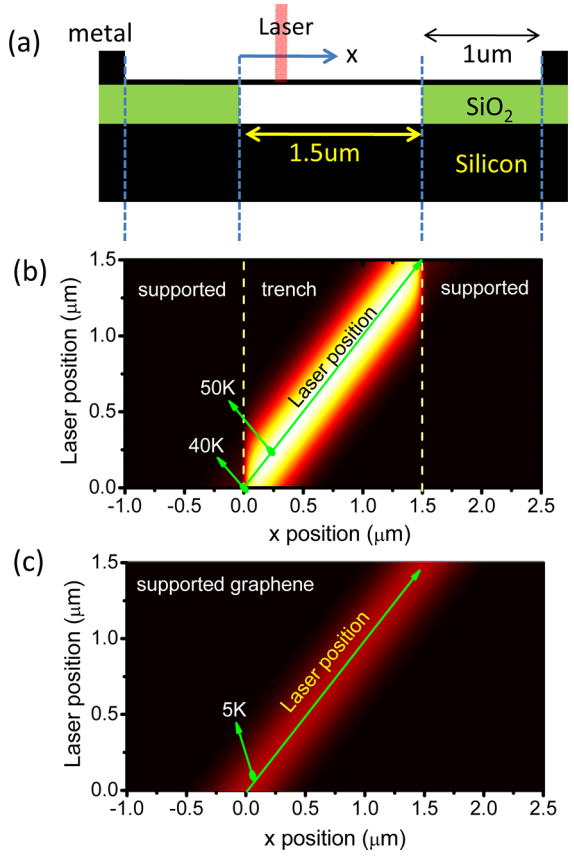

Figure 3. Modeling of the temperature profile. (a) Schematic of the modeled partially suspended device. (b) Intensity plot of the temperature profile for a partially suspended graphene device, i.e., $T_e(x,x_0)$, where x is the transport direction and x_0 is the laser focusing position. (c) Similar to b, except for a fully supported graphene device.

dx.doi.org/10.1021/nl4001037 | Nano Lett. 2013, 13, 1644−1648

the other hand, δT is only $\approx$ 5 K for fully supported graphene devices. Our results are relatively insensitive to the value of κ_e used in this work since $\gamma_e \gg h\kappa_e/L^2$, which implies that the out-of-plane heat flow dominates over the in-plane counterpart. We note that in our analysis, we have ignored the phonon part of the heat conduction, where the lattice temperature is implicitly taken to be at T_0. Contrary to the electronic heat conduction, the phonon's counterpart satisfies $\gamma_{ph} \ll h\kappa_{ph}/L^2$. Due to the much more efficient phonon thermal conductivity, $\kappa_{ph} \sim 3000$ W/m·K,[29] the lattice temperature is only 2.5 Kelvin larger than T_0. This is confirmed by solving an analogous heat equation (i.e., eq 1) for the phonon part assuming an out-of-plane thermal conductance γ_{ph} of 1 MW/m^2·K and 0 MW/m^2·K for the supported[30] and suspended part of graphene.

The photothermoelectric current serves as a "thermometer" of the device's electronic temperature and is given by,

$$I_{TE} \approx \frac{W}{L}\sigma_e \delta T_{junc}(S_t - S_s)\frac{L_{spot}}{W} \tag{3}$$

where σ_e is the electrical conductivity, S is the Seebeck coefficient, and δT_{junc} is the electronic temperature at the electrostatic junction. The transport coefficient σ_e is measured experimentally and can be well fitted to the following formula (note that transport is limited by the lesser doped suspended region),

$$\sigma_e = \frac{\sigma_{min}}{\Delta^{2\alpha}}(E_F^2 + \Delta^2)^{\alpha} \tag{4}$$

where E_F is the Fermi energy of the suspended region, α is a dimensionless number 0.21, Δ is the electron−hole puddle energy, and σ_{min} is the minimum conductivity. Both Δ and σ_{min} can be fitted to the device's electrical conductivity in experiments, while E_F is described by,

$$E_F = \frac{\pi\hbar^2}{2m}n \tag{5}$$

where n is the carrier density and is given by $n = C_B V_G/e + n_0$ where C_B is the gate capacitance and n_0 is the residual fixed charge density. m is the electron's effective mass, which in trilayer graphene is $\approx 0.05 m_e$.[31] Figure 4a shows the device's electrical conductivity fitted to eq 4. The Seebeck coefficient S can then be obtained directly from the Mott formula[32] in conjunction with eq 4. S is plotted in Figure 4b for both the supported (S_s) and the suspended (S_t) part of graphene. The photothermoelectric current, or responsivity, calculated from eq 3 is plotted in Figure 4c, and fitting to the regime of largest responsivity (which is also the regime dominated by the thermoelectric effect) suggests an electronic temperature of δT_{junc} between 35 K and 50 K. We note that the extracted electronic temperature is an order of magnitude larger than what would be expected in supported graphene devices under similar experimental conditions.[3] An overall "negative shift" in the responsivity between the model and experiments in Figure 4c can be accounted for by a finite photovoltaic contribution, caused by the local electric field at the suspended-supported interface.

The extracted temperature is in good agreement with the estimated electronic temperature from solving the heat equation, suggesting that the elimination of a dominant cooling channel via the SPPs can lead to an elevated electronic temperature consistent with the measured photothermoelectric current. Since our device is operating at room temperature, we

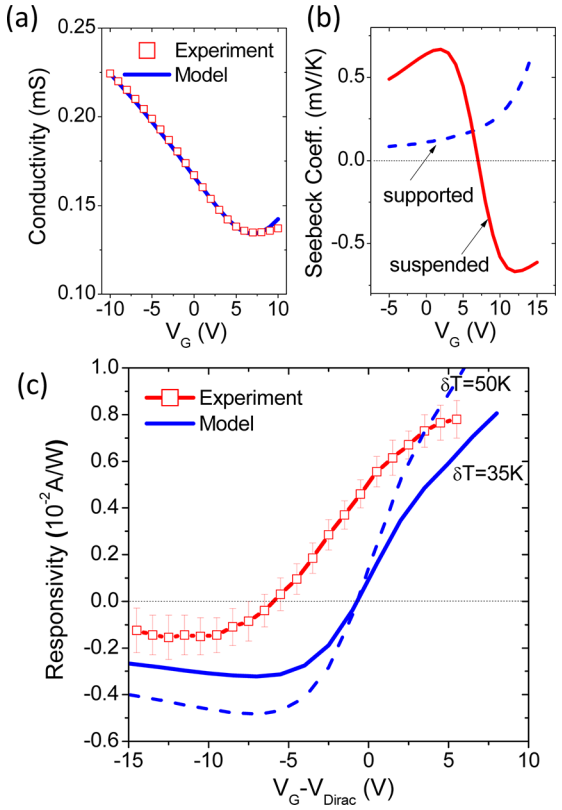

Figure 4. Thermoelectric photocurrent. (a) Electrical characteristic of the partially suspended graphene. The current minimum at 7 V is due to the suspended section. (b) Modeled Seebeck coefficients of the suspended and supported sections. (c) Modeling of the photothermoelectric component of the photocurrent (blue) and comparison with the experiment (red), see main text for details.

expect the electronic cooling to be mainly mediated by the optical phonons, both the internal and extrinsic substrate phonons as accounted for in our above studies. Electronic cooling by acoustic phonon is a significantly less efficient process comparatively. However, impurities could enhance its electronic cooling efficiency via a process known as "super-collision". Recent experiments[21,22] suggest the cooling power associated with this process to be $A((T_0 + \delta T)^3 - T_0^3)$ with A of $\approx$ 1 W·m^{-2}·K^{-3} on supported graphene. Assuming this process to be the main cooling mechanism, our absorbed laser power of 2.8×10^7 W·m^{-2} would then produce an elevated temperature of $\delta T \approx$ 80 K for supported graphene, which is much higher than that extracted from the photothermoelectric current (recall that we obtained $\delta T \approx$ 5 K for supported graphene, Figure 3c). Furthermore, suspending the graphene typically improves the carrier mobility, leading to a smaller rate coefficient A and an even higher estimate for the temperature. Hence, our experiments and analysis strongly suggest that the SPP mechanism is the dominant contribution, which accounts for the photocurrent observed in supported graphene p−n junctions on SiO_2.

In summary, we present in this paper the study of the photocurrent of a suspended graphene device with significantly improved responsivity. The experiment highlights the importance of the phonons of the polar substrate in enhancing the electronic cooling and limiting performance of nonsuspended graphene photodetectors. This study also reinforces the notion that the properties of two-dimensional graphene are strongly

dx.doi.org/10.1021/nl4001037 | Nano Lett. 2013, 13, 1644−1648

influenced by extrinsic factors, pointing to the importance of dielectric engineering for improved graphene photodetector performance.

AUTHOR INFORMATION

Corresponding Author

*E-mail: mfreitag@us.ibm.com

Notes

The authors declare no competing financial interest.

ACKNOWLEDGMENTS

We thank Bruce Ek, Jim Bacchiano, and Zhihong Chen for the sample preparation, and James Tsang, Mathias Steiner, and Hugen Yan for helpful discussions.

REFERENCES

(1) Vora, H.; Kumaravadivel, P.; Nielsen, B.; Du, X. Bolometric response in graphene based superconducting tunnel junctions. *Appl. Phys. Lett.* **2012**, *100*, 153507.

(2) Yan, J.; Kim, M. H.; Elle, J. A.; Sushkov, A. B.; Jenkins, G. S.; Milchberg, H. M.; Fuhrer, M. S.; Drew, H. D. Dual-gated bilayer graphene hot-electron bolometer. *Nat. Nanotechnol.* **2012**, *7*, 472−478.

(3) Freitag, M.; Low, T.; Xia, F.; Avouris, P. Photoconductivity of biased graphene. *Nat. Photonics* **2012**, *7*, 53−59.

(4) Xu, X.; Gabor, N. M.; Alden, J. S.; van der Zande, A. M.; McEuen, P. L. Photo-Thermoelectric Effect at a Graphene Interface Junction. *Nano Lett.* **2009**, *10*, 562−566.

(5) Lemme, M. C.; Koppens, F. H. L.; Falk, A. L.; Rudner, M. S.; Park, H.; Levitov, L. S.; Marcus, C. M. Gate-Activated Photoresponse in a Graphene p−n Junction. *Nano Lett.* **2011**, *11*, 4134−4137.

(6) Gabor, N. M.; Song, J. C. W.; Ma, Q.; Nair, N. L.; Taychatanapat, T.; Watanabe, K.; Taniguchi, T.; Levitov, L. S.; Jarillo-Herrero, P. Hot Carrier-Assisted Intrinsic Photoresponse in Graphene. *Science* **2011**, *334*, 648−652.

(7) Song, J. C. W.; Rudner, M. S.; Marcus, C. M.; Levitov, L. S. Hot Carrier Transport and Photocurrent Response in Graphene. *Nano Lett.* **2011**, *11*, 4688−4692.

(8) Mueller, T.; Xia, F.; Freitag, M.; Tsang, J.; Avouris, P. Role of contacts in graphene transistors: A scanning photocurrent study. *Phys. Rev. B* **2009**, *79*, 245430.

(9) Mueller, T.; Xia, F.; Avouris, P. Graphene photodetectors for high-speed optical communications. *Nat. Photonics* **2010**, *4*, 297−301.

(10) Peters, E. C.; Lee, E. J.; Burghard, M.; Kern, K. Gate dependent photocurrents at a graphene p−n junction. *Appl. Phys. Lett.* **2010**, *97*, 193102.

(11) Rao, G.; Freitag, M.; Chiu, H.-Y.; Sundaram, R. S.; Avouris, P. Raman and Photocurrent Imaging of Electrical Stress-Induced p−n Junctions in Graphene. *ACS Nano* **2011**, *5*, 5848−5854.

(12) Urich, A.; Unterrainer, K.; Mueller, T. Intrinsic Response Time of Graphene Photodetectors. *Nano Lett.* **2011**, *11*, 2804−2808.

(13) Sun, D.; Aivazian, G.; Jones, A. M.; Ross, J. S.; Yao, W.; Cobden, D.; Xu, X. Ultrafast hot-carrier-dominated photocurrent in graphene. *Nat. Nanotechnol.* **2012**, *7*, 114−118.

(14) Schaller, R. D.; Klimov, V. I. High Efficiency Carrier Multiplication in PbSe Nanocrystals: Implications for Solar Energy Conversion. *Phys. Rev. Lett.* **2004**, *92*, 186601.

(15) Wellstood, F. C.; Urbina, C.; Clarke, J. Hot-electron effects in metals. *Phys. Rev. B* **1994**, *49*, 5942−5955.

(16) Efetov, D. K.; Kim, P. Controlling Electron-Phonon Interactions in Graphene at Ultrahigh Carrier Densities. *Phys. Rev. Lett.* **2010**, *105*, 256805.

(17) Bistritzer, R.; MacDonald, A. H. Electronic Cooling in Graphene. *Phys. Rev. Lett.* **2009**, *102*, 206410.

(18) Tse, W.-K.; Das Sarma, S. Energy relaxation of hot Dirac fermions in graphene. *Phys. Rev. B* **2009**, *79*, 235406.

(19) Ulstrup, S.; Bianchi, M.; Hatch, R.; Guan, D.; Baraldi, A.; Alfè, D.; Hornekær, L.; Hofmann, P. High-temperature behaviour of supported graphene: electron-phonon coupling and substrate-induced doping. *arXiv:1203.2187v1* [cond-mat.mes-hall], **2012**.

(20) Betz, A. C.; Vialla, F.; Brunel, D.; Voisin, C.; Picher, M.; Cavanna, A.; Madouri, A.; Feve, G.; Berroir, J. M.; Placais, B.; et al. Hot Electron Cooling by Acoustic Phonons in Graphene. *Phys. Rev. Lett.* **2012**, *109*, 056805.

(21) Graham, M. W.; Shi, S.-F.; Ralph, D. C.; Park, J.; McEuen, P. L. Photocurrent measurements of supercollision cooling in graphene. *Nat. Phys.* **2012**, *9*, 103−108.

(22) Betz, A. C.; Jhang, S. H.; Pallecchi, E.; Ferreira, R.; Feve, G.; Berroir, J. M.; Placais, B. Supercollision cooling in undoped graphene. *Nat. Phys.* **2012**, *9*, 109−112.

(23) Perebeinos, V.; Rotkin, S. V.; Petrov, A. G.; Avouris, P. The Effects of Substrate Phonon Mode Scattering on Transport in Carbon Nanotubes. *Nano Lett.* **2008**, *9*, 312−316.

(24) Rotkin, S. V.; Perebeinos, V.; Petrov, A. G.; Avouris, P. An Essential Mechanism of Heat Dissipation in Carbon Nanotube Electronics. *Nano Lett.* **2009**, *9*, 1850−1855.

(25) Low, T.; Perebeinos, V.; Kim, R.; Freitag, M.; Avouris, P. Cooling of photoexcited carriers in graphene by internal and substrate phonons. *Phys. Rev. B* **2012**, *86*, 045413.

(26) Yan, H.; Xia, F.; Li, Z.; Avouris, P. Plasmonics of coupled graphene micro-structures. *arXiv:1205.6841* [cond-mat.mes-hall], **2012**.

(27) Moser, J.; Barreiro, A.; Bachtold, A. Current-induced cleaning of graphene. *Appl. Phys. Lett.* **2007**, *91*, 163513−3.

(28) Volokitin, A. I.; Persson, B. N. J. Near-field radiative heat transfer between closely spaced graphene and amorphous SiO_2. *Phys. Rev. B* **2011**, *83*, 241407.

(29) Chen, S.; Wu, Q.; Mishra, C.; Kang, J.; Zhang, H.; Cho, K.; Cai, W.; Balandin, A. A.; Ruoff, R. S. Thermal conductivity of isotopically modified graphene. *Nat. Mater.* **2012**, *11*, 203−207.

(30) Freitag, M.; Steiner, M.; Martin, Y.; Perebeinos, V.; Chen, Z.; Tsang, J. C.; Avouris, P. Energy Dissipation in Graphene Field-Effect Transistors. *Nano Lett.* **2009**, *9*, 1883−1888.

(31) Craciun, M. F.; Russo, S.; Yamamoto, M.; Oostinga, J. B.; Morpurgo, A. F.; Tarucha, S. Trilayer graphene is a semimetal with a gate-tunable band overlap. *Nat. Nanotechnol.* **2009**, *4*, 383−388.

(32) Cutler, M.; Mott, N. F. Observation of Anderson Localization in an Electron Gas. *Phys. Rev.* **1969**, *181*, 1336−1340.